Chapter 8

Generator Insulation-Aging On-Line Monitoring Technique Based on Fiber Optic Detecting Technology

Peter Kung

Additional information is available at the end of the chapter

http://dx.doi.org/10.5772/intechopen.78065

Abstract

The relationship between insulation aging and generator lifespan using fiber optic sensors (FOSs) is explored to ultimately improve asset lifespan through smart choices in running conditions and maintenance. Insulation aging is a major factor that causes generator failure. FOS provides the rare opportunity of being installed up close to the insulation, monitoring degradations that are otherwise difficult to detect. FOSs, unlike purely electrical transducers, are immune to high voltage (HV) and strong electromagnetic (EM) fields. They are small and have a proven long life by their deployment in the Telecom industry. The proposed FOS is a Fabry-Perot cavity made up of two identical fiber Bragg gratings (FBGs) using light wave interference as the working principle. Such architecture delivers simultaneous vibration (10 Hz–1 kHz) and temperature (0.1°C resolution) monitoring, both helping to spot irregular vibration patterns (signatures) and hot-spots inside the generator stator slots. The signal processing unit equipped with a gateway device can help to connect the large volume of sensor data, allowing correlation with the supervisory control and data acquisition (SCADA) system data of the plant. This chapter also elaborates on the field test jointly conducted with Calpine Corporation and Oz Optics, Ltd. (Ottawa, Ontario, Canada).

Keywords: hot-spot, fiber Bragg grating (FBG), Brillouin scattering, generator, vibration, Fiber optic

1. Introduction

Insulation aging phenomenon in air-cooled gas-fired generators is a problem confronting both original equipment manufacturers (OEMs) and owners of these competitive assets [1]. The expected life of these generators largely depends on design, manufacturing workmanship and choice of material. It also depends on the way they are used. They are used to

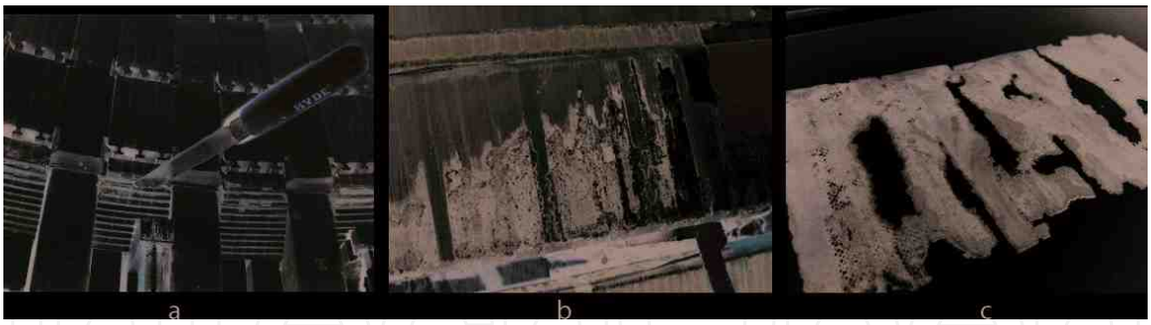

Figure 1. At the left, local loose core found using simple knife check. At the middle, defects start to appear as pinholes. At the right, partial discharge removes the conducting paint without affecting the underlying mica.

adapt to the intermittent nature of renewable energies, subjecting them to many start-stop cycles. Such cycles give rise to stresses and creeps from material expansion and contraction. Under constant cost reduction, pressure generators are getting less expensive and their quality also suffers. Their characteristic strong vibrations that shake the structure loose further aggravate this.

Figure 1 (left) shows how vibration causes delamination in the core, allowing the varnish to wear out and then eddy currents to introduce hot-spots affecting the performance of the winding in the slot located close by. It becomes a downward spiral of mechanical degradation. Some of the cost reducing innovations that were previously introduced worked well in a base load operation. However, in a constant start-stop mode of operation, generators are susceptible to outage early in their life because they are air-cooled. The constant thermal cycling combined with the variable characteristics of the air contribute to early wear. They can suffer from a new failure mode called vibration sparking. This is the first time that this failure mechanism has been observed as failure in progress as shown in **Figure 1** (middle). They usually become uncovered upon a complete breakdown. A simple model that combines thermal aging and a mechanical vibration-assisted degradation process is introduced in the following sections.

Thermal aging of the insulation is often related to temperature as generators have been around for more than 100 years. The insulation material has gone through many innovative improvements [2]. A greater focus is given on the mica material and winding design that has a top layer of conductive carbon paint or conductive tape, which makes connection to the grounded stator. This is the working principle of the generator and other rotating machines such as the large industrial motors.

2. Insulation aging

The investigation result of generator fault event shows that the failure probability of the single generator will be increasing with the generator's capacity and applying time increasing. The investigation results show that more than 50% electrical equipment failures are caused by the insulation system [3]. How to detect generator insulation aging and degradation is of great economic and social significance. Improved reliability in power distribution affects every level of society.

http://dx.doi.org/10.5772/intechopen.78065

2.1. Insulation aging reasons

For the gas-fired generator, the stator winding, which is the direct carrier that generates electricity, would sustain different kinds of combined effects in the process of operation simultaneously, such as electric, heat, mechanical and any other actions [4]. The investigation and researching results gained by many researchers, show that a series of physical and chemical changes will occur during the insulation materials operating for a long time, such as insulation medium softening, pinhole, cracking, ionization, etc. [5]. It is generally assumed that insulation aging is affected mainly by thermal cycling, heat aging, electric aging, mechanical vibration aging combined together [6].

2.1.1. Heat-aging effect

Many generator insulation materials consist of mica and epoxides. Mica and epoxides both have excellent heat resistant characteristics. The occurring rate of the aging phenomenon is slow while the generator is working under normal temperatures, and the higher the temperature of the insulating material is, the faster the heat aging. The insulation materials performance decreases with the increase of temperature. For the generator, the main reasons for the increase of insulation temperature are the resistance heat of the conductor, partial discharge, leakage current of the insulation and the heat caused by the dielectric loss. For the epoxide-mica insulation medium, there are two ways to affect the insulation performance: one is the epoxy-mica temper embrittlement and thermal degradation and another is the local defects caused by thermal expansion of the polymer [7].

2.1.2. Mechanical stress effect

The generator stator windings are nested in the mechanical supporting structure. The stator winding is generally running under mechanical stress. At the same time, there always exists vibration, which corresponds with stress. The electromagnetic force generated on the stator windings changes the rotor turning speed variation. Due to the effect of long time fluctuating mechanical force, there would produce some joint loosening and vibration. Under the action of alternating stress and vibration, the conductive carbon coating attached to insulation material would loosen and shed because of the vibration fatigue. We call it mechanical insulation aging which is caused by mechanical stress. The alternating mechanical force comes from static mechanical force, the start-stop electromagnetic force, and mechanical vibration force at running time [8]. Mechanical vibration force at running time produces as illustrated in **Figure 2**.

2.1.3. Sparking effect

The winding insulation of generators are made of epoxy & mica combined together. Due to the difference of expansion coefficient and manufacturing process, there exists some micro-gaps between materials and carbon coating, different insulation layers, under the effect of electric field, the sparking caused by partial discharge would be showing up at the micro-gap location. Due to the sparking, there are three damage types. One type is that the main insulation thickness becomes thinner because the adhesive between the coating and the insulation medium is carbonized by the high temperature in the micro-gap caused by the partial discharge. The second type is that the edges of the insulation medium and the air gap wall

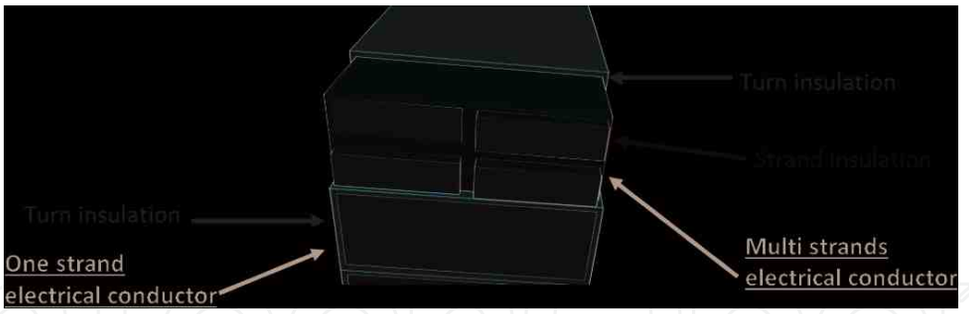

Figure 2. Mechanical vibration force at running time produces illustrated. Courtesy of QPS Photronics.

would appear to erode into pit and pinhole defects because of the striking by a large number of charged particles at high speed, which lead to a decline in insulation. The third type is that the discharge can produce ozone, which damages the insulation and copper conductor by combining with water, NO and NO_2 [9–15].

2.2. Gas-fired generator aging

2.2.1. Insulation thermal aging

The reliability of the insulation is dependent on the thickness of the mica layer being applied in different parts of the windings [16–18] as illustrated in **Figure 3**.

Then, a top coating of conductive layer is overlaid to complete the structure. Therefore, the full voltage will now be exercised across the insulation as depicted in **Figure 4**.

The layers are quite thick, normally free of pinholes, defects, and other imperfections. However, the material ages with time, which results in reduction of their insulation properties. Defects start to form from partial discharge (PD) occurring where the windings show traces of contamination left behind during manufacturing and handling. This phenomenon is one among other degradation processes at work.

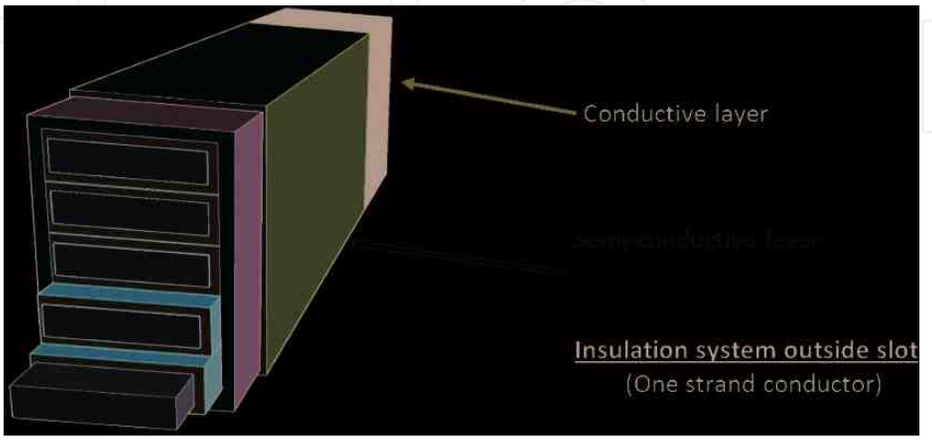

Figure 3. Conceptual depiction of the various insulation subdivisions. Courtesy of QPS Photronics.

http://dx.doi.org/10.5772/intechopen.78065

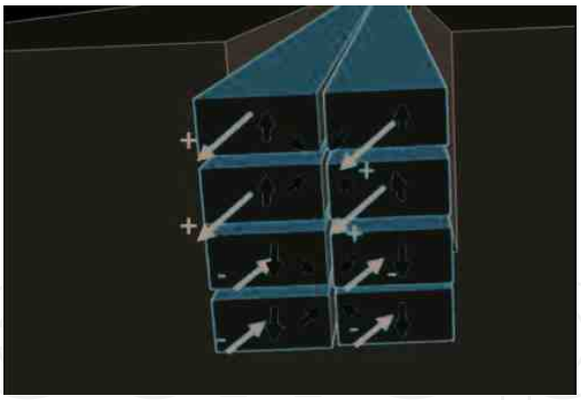

Figure 4. Depiction of grounded conductive outermost layer. Courtesy of QPS Photronics.

2.2.2. Strong vibration aging

Vibration is an equally powerful aging mechanism. Vibration is inherent in the design structure of any rotating machine. Most generators are two-pole machines where uneven air gaps can be introduced due to misalignment, giving rise to a two-time line frequency (2xLF) nominal signature [19]. Then there is the effect of unbalancing, which gives a strong line frequency (1xLF) component. Vibration can become much stronger when the material and structure become close to a resonance mode. Excessive vibration can start rubbing the insulation, triggering shortened turns or shorts to ground. **Figure 5** shows the interactions inside a complex winding. Vibration in a generator can occur in both the radial and tangential directions.

2.2.3. Hot-spot vibration sparking aging

Vibration sparking is a special process in gas-fired generators combining insulation thermal aging together with strong vibration effects [20–22]. Hot-spot measurement was performed in a random wound electric machine coil [23]. Vibration measurement was also performed

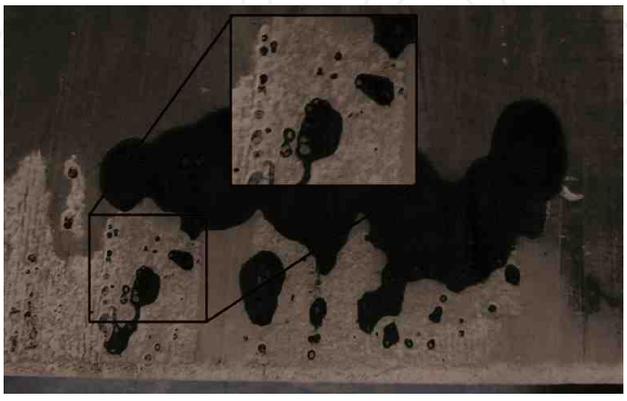

Figure 5. Eight strands within a stator slot interacting with each other under the effect of vibration. Courtesy of QPS Photronics.

using a wideband fiber optic vibration sensor (see [21]). For confirming the effect of vibration sparking on insulation performance, some methods were actually developed to monitor the end winding of a large power generator. For example, a simple fiber Bragg grating (FBG) have been used to measure hot-spots and they found the measured value affected by vibration of the motor (see [23]). A thin vibration sensor was developed for monitoring winding vibration inside the transformer [24] by making use of the long gauge effect, namely a length of single-mode fiber spliced onto the cavity rendered the whole fiber a distributed vibration sensor. Meanwhile, the field test was performed in cooperation with Calpine Corporation. When Calpine Corporation found signs of disturbance in the winding insulation, they realized that it was time to perform a major maintenance, leading to a rewind. Some samples of the affected windings were examined (**Figure 6**). There seems to be various stages of degradation.

All the measurement research above shows that as the revolutions per minute (RPM) are increased, various local resonances started to appear. Then, unique frequency signatures

Figure 6. Patches of insulation damage on winding. Close-up highlights pinholes formed in the conductive carbon paint. Courtesy of QPS Photronics and Calpine Corporation.

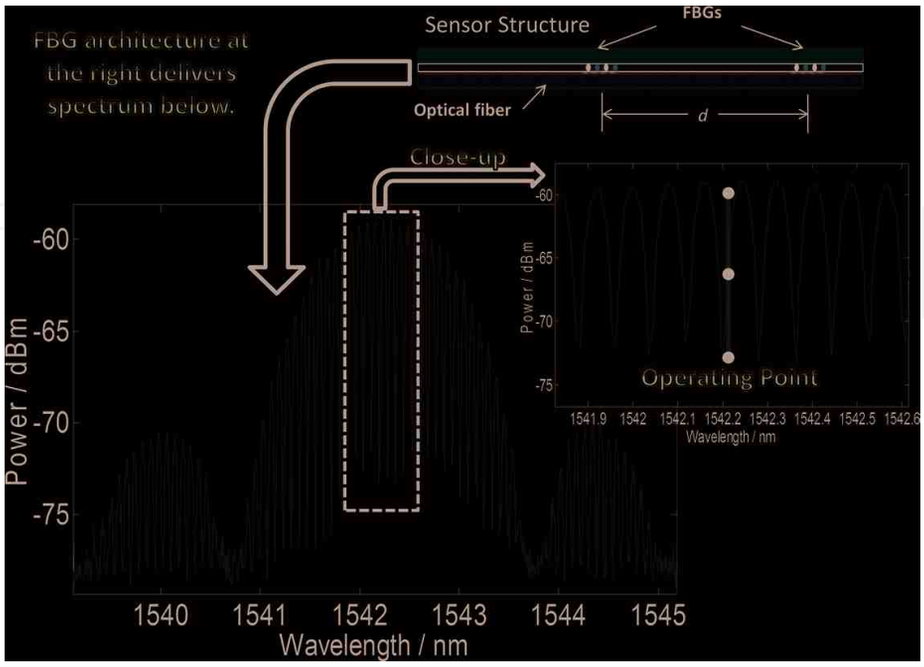

Figure 7. At left, conceptualization of vibration sparking. At right, complete winding insulation became destroyed at another power plant suspected of having similar problem.

appeared and were associated with different deliberately introduced faults like open-circuits, short-circuits, and bearing digs. Note that they are recoverable after the experiment. It is observed that they are very distinct from those obtained when the motor was restored to its original healthy condition (see [19]).

It is hypothesized these were related hot-spots developed in the stator, caused by eddy current loops, formed when damage occurs between the insulation and the neighboring laminated steel plate. The hot-spots reduced the performance of the insulation and PD subsequently occurred, eroding further the carbon paint. Furthermore, mica insulation also suffered from damage. PD activities would not have sufficient energy to puncture the mica and another failure mechanism might be at work, vibration sparking. Such process is defined by excessive vibration occurring in the slot so that the carbon paint, normally maintaining ground contact to the stator, failed and HV appears at some of those disturbed locations and the air breaks down to form a plasma. **Figure 7** (left) illustrates the concept. For the other side of the vibrating part, the plasma lost contact with its current source. This is a powerful source of electro-etching, an industrial process used to etch hard material like ceramics. If this process continues undetected, it destroys the mica insulation, leading to an unplanned outage as shown in **Figure 7** (right).

3. Insulation aging detection theory

3.1. Insulation aging model

In order to master the law of aging and reduce the losses due to aging, some aging models of insulation have been established based on practical experience and theoretical analysis.

3.1.1. The aging model of single factor

(1) Electric stress aging model

The Power Reciprocal model in low electric field and the Index model in high electric field are proposed based on a lot of electric stress affected researches. The Power Reciprocal model is as follows [25]:

$$L = kE^{-n} \tag{1}$$

where: L represents failure time, E represents external applied voltage, k and n are empirical constants.

The Index model is as follows [26]:

$$L = a\exp(-bE) \tag{2}$$

where: L represents failure time, E represents external applied voltage, a and b are empirical constants.

(2) Thermal aging model

The thermal aging model based on the equation that describing the relationship between the rate constant of the chemical reaction and the temperature as follows:

$$\ln t = \ln A + \frac{E_0}{RT} \tag{3}$$

where: t represents the set testing time, A is constant, E_0 represents the energy loss during the process of aging (unit: kJ/mol), R equals to the gas constant (8.314 J/mol·K), T represents temperature (K).

(3) Mechanical stress aging model

The mechanical stress aging model of a large motor is generally expressed by the empirical formula as follows:

$$L = K_m S^{-m} \tag{4}$$

where: L represents the failure time, S represents the mechanical stress, m and K are empirical constants related to vibration frequency [27].

3.1.2. Electric-thermal two-factor aging model

With the in-depth study of single factor electric and thermal aging, it is found that the reasons for the insulation aging are not isolated. The electric-thermal two-factor aging model that is widely accepted is as follows:

(1) Simoni model

Based on the function of hypothetical electric field $F(E) = \ln(E/E_0)$, Simoni proposed the two-factor aging model as follows:

$$L(T, E) = L_0 \left(\frac{E}{E_0}\right)^{-A} \exp\left[-B\Delta\left(\frac{1}{T}\right)\right] \tag{5}$$

where: $A = n - b\Delta(1/T)$, n represents the index of the power reciprocal, L_0 represents the break-down time at $E = E_0$, E represents applied electric-field, E_0 represents a reference electric-field value, b represents an empirical constant determined by the insulation materials, B represents the constant of the single factor thermal aging model, T represents the temperature (K).

(2) Ramu model

Based on the rate of Eyring physical chemistry reaction and considering the temperature function as constant, the Ramu the model is established from the Power Reciprocal aging model as follows [28]:

$$L(T, E) = c(T)\, E^{-n(T)} \exp\left[-B\Delta\left(\frac{1}{T}\right)\right] \tag{6}$$

where: parameter definitions are identical as the ones found in the Simoni model, c and n are empirical constants.

http://dx.doi.org/10.5772/intechopen.78065

(3) Crine model

Crine proposed that the process of aging could be characterized by the energy barrier, and considered that the age of the insulation medium equals the time of the charged particles crossing the barrier. Based on the hypothesis that the average time of collective carriers through the potential barrier are equal to the time of a single carrier passing through the barrier, the aging model described by the relation of thermal-dynamic is obtained as follows:

$$L = \frac{h}{kT}\exp\left[\frac{\Delta G - e\lambda E}{kT}\right] \tag{7}$$

where: L represents the failure time, h represents the Plank constant, k represents Pohl Seidman constant, ΔG represents free energy, λ represents the width of barrier, and e represents the particle charge involved in the aging process.

The mathematical models of insulation aging above show how to theoretically predict the temperature, PD and stress in a timely fashion. It is the foundation of predicting the life of insulation materials and reducing safety accidents. In the context of the demand for electric power equipment that goes increasingly up, researchers nowadays have their full attention on predictive methods to trend the aging of insulation and therefore predict the generator's service life.

3.2. Fiber grating detection technology

Due to the complex environment caused by electricity, heat, machinery and chemistry, there are few sensors able to detect the insulation's aging in generators. With the increasing sophistication of fiber optic based technology, FBG based sensor has become the research focus in the field of sensors because of its inherent advantages, such as compact structure, corrosion resistance, intrinsic passivity, indifference to electromagnetic interference and its multiplexing abilities.

3.2.1. Principle of optical Fiber sensing technology

Optical fiber sensing technology senses and transmits external environment parameter variations based on the optical fiber medium. The optical fiber has the characteristic and ability to sense and transmit the information to the optical-electric field in itself directly or indirectly. When a beam of light illuminates through optical fiber, the change of the external environment parameters (e.g. vibration) could be sensed. The optical-electric fields characteristic value in the optical fiber, such as amplitude, phase, wavelength and polarization, would be affected by the signals sensed while the sensed signal propagates in the fiber. Furthermore, by using a demodulation device, the changes of the external environment physical parameters quantity could be obtained by using the signal reversing method [29]. The principle of optical fiber sensing is depicted in **Figure 8**.

3.2.2. Fiber Bragg grating sensor model

Based on the light coupling-mode theory at the scale of micro-disturbances, the effective refractive index of grating region and the central wavelength of FBG could be obtained by solving the light equation as follows [29]:

$$\delta n_{eff} = \overline{\delta n_{eff}} \left[1 + \cos\left(\frac{2\pi}{\Lambda} z\right)\right] \tag{8}$$

where: n_{eff} represents the effect refractive index, Λ represents grating period, $\overline{\delta n_{eff}}$ represents the change of the average effective refractive index.

The characteristic wavelength that interacts with the optical fiber corrugation is represented by:

$$\lambda_B = 2\, n_{eff} \Lambda \tag{9}$$

where: λ_B represents the Bragg (central) wavelength.

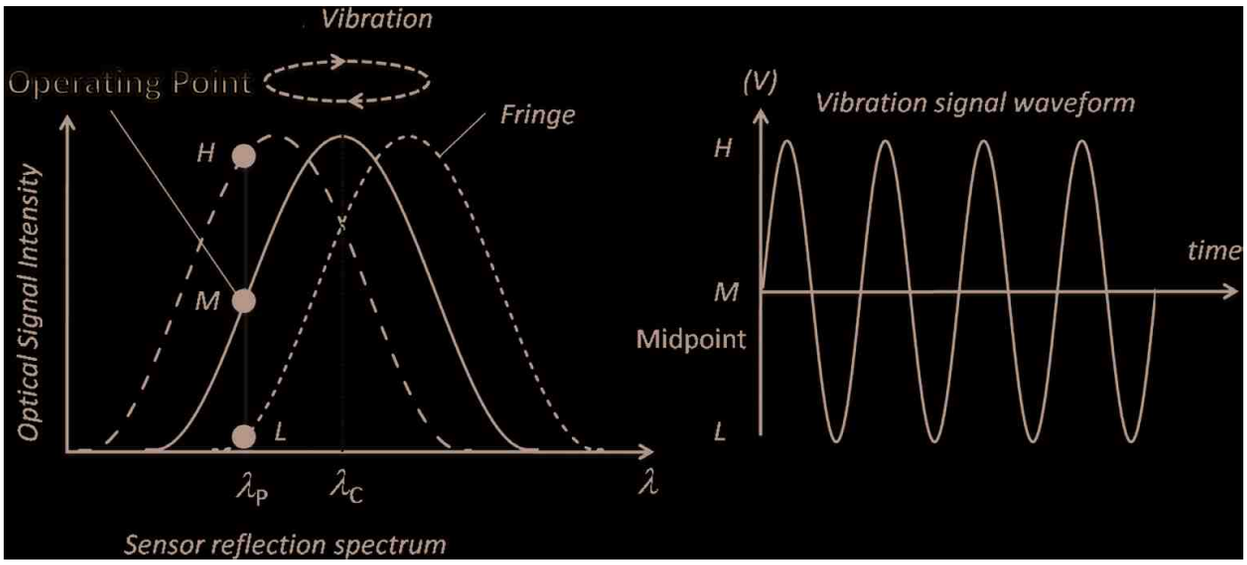

Figure 8. The principle of optical fiber sensing.

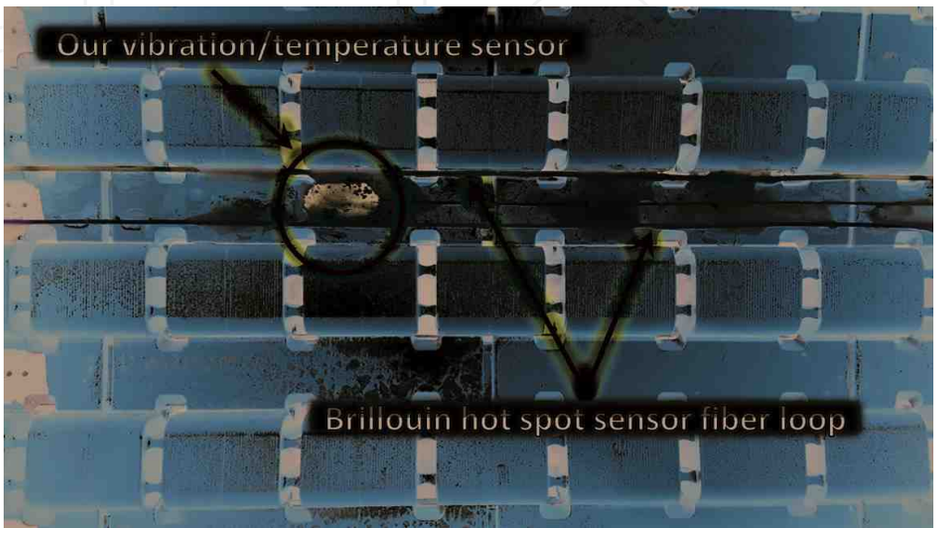

Figure 9. The frame of the Bragg fiber grating and its reflecting schematic diagram. Courtesy of QPS Photronics.

http://dx.doi.org/10.5772/intechopen.78065

From the FBG central wavelength formula, we can conclude that: (A) when a beam of incident light transmits through the grating region, there always exists a fraction of the light that reflects back, and the wavelength of the reflected light must satisfy the Bragg wavelength Eq. (9); (B) The Bragg wavelength of the FBG only depends on the grating period Λ and the refractive index n_{eff}.

A proper FBG will have its central wavelength solely determined by the corrugation period and effective refractive index. The FBG central wavelength, period, and effective refractive index are all fixed constants, meaning that the reflection spectrum of the FBG central wavelength is always fixed at reflecting peak on the condition that the FBG sensor is under the same environmental conditions [30, 31]. The frame of the FBG and its reflecting schematic diagram are shown in **Figure 9**.

3.2.3. Fiber Bragg grating sensor model for temperature

Due to the central wavelength shifted with the change of temperature, based on the formula (9) and the assumption that the fiber grating is only affected by the temperature, the central wavelength shifting value of the FBG could be obtained as follows:

$$\frac{\Delta\lambda_B}{\lambda_B} = (\alpha_s + \zeta_s)\Delta T \tag{10}$$

where: $\alpha_s = (1/\Lambda)(\Delta\Lambda/\Delta T)$ represents the fiber's thermal expansion coefficient, and is used to describe the grating pitch variation with the temperature. $\zeta_s = (1/n_{eff})(\Delta n_{eff}/\Delta T)$ represents the FBG thermo-optical coefficient, and is used to describe the variation of the material refractive index changing with the temperature.

Based on the Eq. (10), the variation of the ambient temperature could be reversed by detecting the variation of the central wavelength $\Delta\lambda_B$.

3.2.4. Fiber Bragg grating sensor model for vibration

Due to principle of the fiber grating pitch and refractive index that vary with the fiber undergoing strain along the axial direction, based on the central wavelength formula (9) and the assumption that the fiber grating is only affected by it, the central wavelength shifting value of the Bragg fiber grating could be obtained as follows:

$$\frac{\Delta\lambda_B}{\lambda_B} = \frac{\Delta\Lambda}{\Lambda} + \frac{\Delta n_{eff}}{n_{eff}} \tag{11}$$

where: $\Delta\lambda_B$, $\Delta\Lambda$ and Δn_{eff} represent the changing value of FBG central wavelength, grating period and refractive index separately.

When strain is applied along the axial direction in the fiber, the refractive index variation of the FBG satisfies the following formula:

$$\frac{\Delta n_{eff}}{n_{eff}} = \frac{1}{2} n_{eff}^2 \left[(1-\mu) P_{12} - \mu P_{11}\right] \varepsilon = -P_e \varepsilon \tag{12}$$

where: P_e represents the elasto-optical coefficient, and defined as $P_e = n_{eff}^2[(1-\mu)P_{12} - \mu P_{11}]/2$, ε represents strain of the fiber grating along the axial direction, μ represents the Poisson's ratio of the fiber material. P_{11} and P_{12} represent the elastic tensor components of the fiber grating.

Based on the definition of axial strain and Eq. (11), we could obtain the strain detecting formula as follows:

$$\frac{\Delta\lambda_B}{\lambda_B} = (1 - P_e)\varepsilon$$

Based on the relationship between strain and wavelength and the detecting value of the center wavelength, the vibration could be reversed by using the relationship between stress and strain.

3.3. Long-gauge vibration/temperature sensor

3.3.1. Introduction to QPS Photronics

QPS is an innovator in the field of fiber optic sensors and specifically FBG's. They bring gratings from research into marketable products.

3.3.2. Introduction of long-gauge vibration/temperature sensor

Because fiber optics are made of glass with no conducting materials, fitting well in environments undergoing high-voltages and strong electromagnetic fields, based on the FBG vibration/temperature sensor model, this section introduces how the sensors were designed to satisfy the power industry requirements using FBGs.

The ability to measure both vibration and temperature is based on interference: two identical FBGs are printed on the same fiber at a small distance, which forms a cavity. When a laser beam with matching center wavelength is emitted into the cavity, it is reflected and goes through a 180° phase shift, giving rise to two interfering beams and a dense fringe spectrum as shown in **Figure 10**.

The larger the cavity length, the denser will be the fringe pack with steeper slope, playing on sensitivity. The vibration function is realized by programming an operating point at the midpoint of the rising slope of a selected fringe. This operating point stays locked using

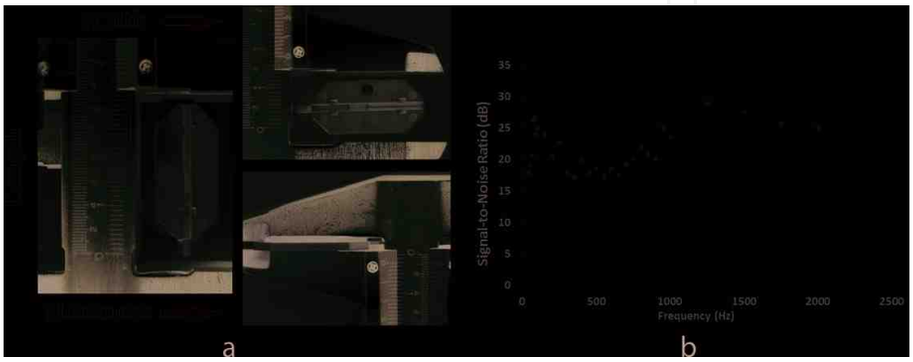

Figure 10. Correlation between fiber optic structure and resulting spectrum where a selected fringe will be monitored for changes due to both static/dynamic strain and temperature. Courtesy of QPS Photronics.

http://dx.doi.org/10.5772/intechopen.78065

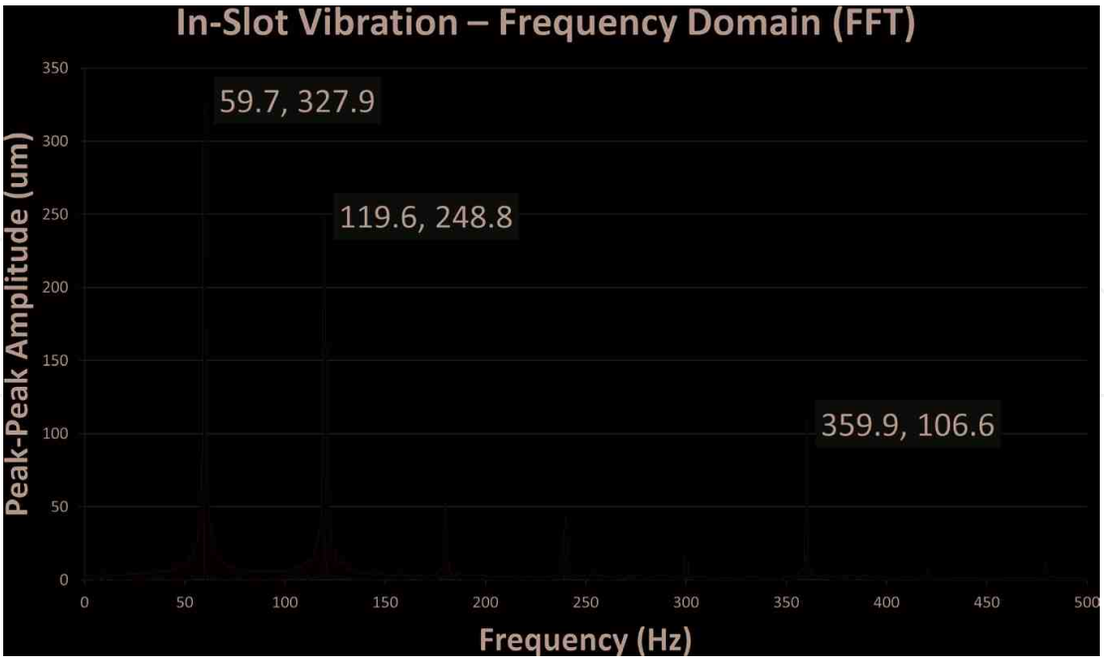

Figure 11. Correspondence between fringe oscillation and resulting vibration. Courtesy of QPS Photronics.

both the laser current (LC) and the thermoelectric cooler (TEC) analog controls of the laser. When vibration occurs, the fringe pattern will be moving right and left, it forces the operating point to ride up and down the slope, translated into linear intensity changes. The changes accurately reflect the actual vibration that is occurring. Since the cavity is also affected by temperature, a self-calibration algorithm was introduced to re-establish the operating point and such compensation delivers an indirect method to measure temperature (see **Figure 11**).

Another invention linked to the cavity is the long gauge technology. By splicing a length of single-mode optical fiber on to the cavity, a new cavity sprouts between the two matching FBGs cavity and the interrogation system connector. Said connector triggers a Fresnel broadband reflection, enabling a thin in-slot vibration distributed sensor to be used in a field test inside a gas-fired generator [32]. The FBG based architecture is housed within a 2 mm thin package that allows easy insertion into tight spots, whereas another supplier of the same field requires two separate large sensors that limit locations where they could be installed [33].

4. Sensing temperature and vibration

Based on the system for temperature and vibration monitoring shown in **Figure 12**, the generator insulation's temperature and vibration becomes possible by using different sensing units that are placed at different locations. By control and analyzing different signals received from different sensors, not only the insulation temperature and vibration can be obtained, but insulation hot-spots can be pinpointed by using the relation between wavelength and vibration.

The detecting system consists of three parts: the signal control & processing unit, signal transmission unit and sensing unit. After the output of the optical signal is converted into an electrical equivalent by the photoelectric converter, and acquired & collected by the data collecting

system, the signal can be transmitted to the computer and processed by the specific software. Then the hot-spot/temperature and vibration can be determined. The related parameters of the vibration of the measured object can be obtained after the analysis and processing of the data on the computer through the vibration monitoring software. The signal control & processing unit consists of an incident optical source, interrogator, display and computer. Incident optical source is used as the stimulating source of the incident light, computer that installed the control software was considered as the head of the detecting system and could send the information and analyze the feedback signal that come from the interrogator complete.

In order to get more information of different locations in the insulation, several fiber gratings having different center wavelength are set in different locations of the optical fiber. Many optical fibers are connected to the interrogator and form the sensing transducer array. The system of the temperature and vibration detection is shown as **Figure 12** and the sensing transducer array is shown as **Figure 13**.

4.1. Details of the field test

There are two types of sensors. One of them makes use of the Brillouin technology where two laser beams are fed into the same fiber optic loop and both lasers have very close center wavelengths that are made to beat against each other, generating a beat frequency. This beat frequency is sensitive to any index changes in the fiber as hot spots. Hence, it is able to report their location along the sensing fiber. The temperature sensor forms a loop inside the slot. In the middle of it a single point temperature (yet distributed for vibration) sensor is installed (see **Figure 14**). The top slightly bluish fiber together with the bottom yellow fiber are the Brillouin temperature sensing loop; the dark hexagon houses the temperature sensing cavity with vibration sensitivity for the whole length of the fiber extension. The whole length of the slot, which measures five meters long, has its vibration captured. The single point temperature measurement provides a temperature reference for the Brillouin hot spot temperature sensing measurement.

Besides the Brillouin hot spots sensor and the in-slot vibration sensor, two other cavity vibration sensors were installed. One is coupled with the end winding lead and another one with the end winding bus, all are done on the neutral phase of the generator. All sensing fibers

Figure 12. System diagram for temperature and vibration detection. Courtesy of QPS Photronics.

are protected by Teflon tubes where the sensor tip is housed in a molded PEEK package as shown in **Figure 15** (left). It is an open face design. The same sensor was also used to measure vibration inside the transformer. The long gauge vibration sensor is a wideband sensor, able to detect frequencies ranging from 10 Hz to 1 kHz for standard version and 5 Hz to 2 kHz for extended sensing range as depicted in **Figure 15** (right).

4.2. Vibration sensing

4.2.1. In-slot vibration

Gas-fired generators are known to produce strong vibration and noise [34]. The in-slot vibration sensor, which has been installed onto the wedge (see **Figure 14**), gave a very clear vibration response as illustrated in **Figure 16**.

We observed a strong line frequency (1xLF) vibration peak together with a strong two times line frequency (2xLF) component. The 1xLF component measures 15-mil peak-to-peak and the 2xLF component measured 10-mil peak-to-peak. This was very high compared with

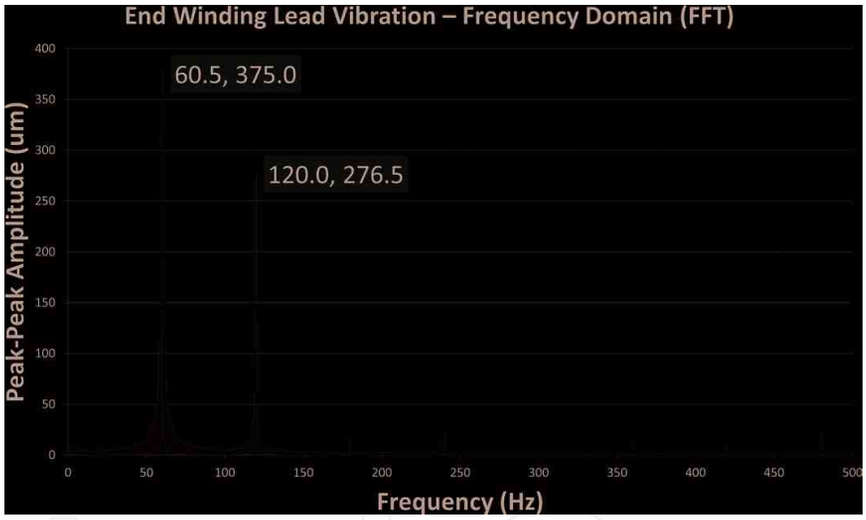

Figure 13. The sensing transducer array. Courtesy of QPS Photronics.

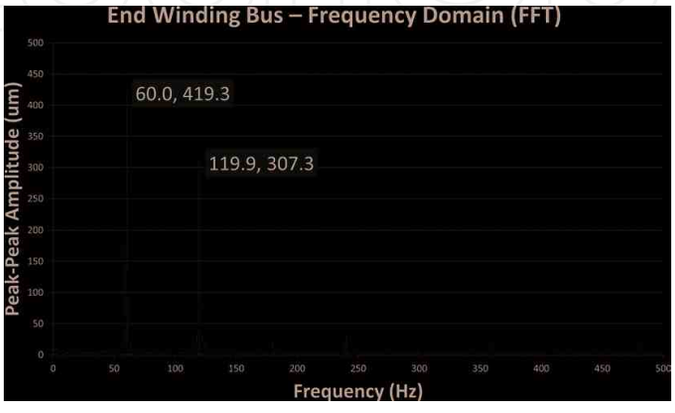

Figure 14. The in-slot vibration sensor installed between the Brillouin temperature sensing fiber loop (U-turn not shown). Courtesy of Calpine Corporation and QPS Photronics.

previously experienced 6-mil peak-to-peak in the end winding vibration of coal-fired generators. It is noted that there exists some harmonics, which rolled off normally but then showed a strong peak at 6xLF. In this generator design, the bearing is coupled onto the frame, which became incorporated into the slot vibration. Concern was expressed to Calpine as this seems to be slightly too high. The 1xLF vibration seems to be related to balancing while the 2xLF component to alignment. This excessive vibration appears to validate the visual inspection of the winding sample cutout from the generator before the rewind.

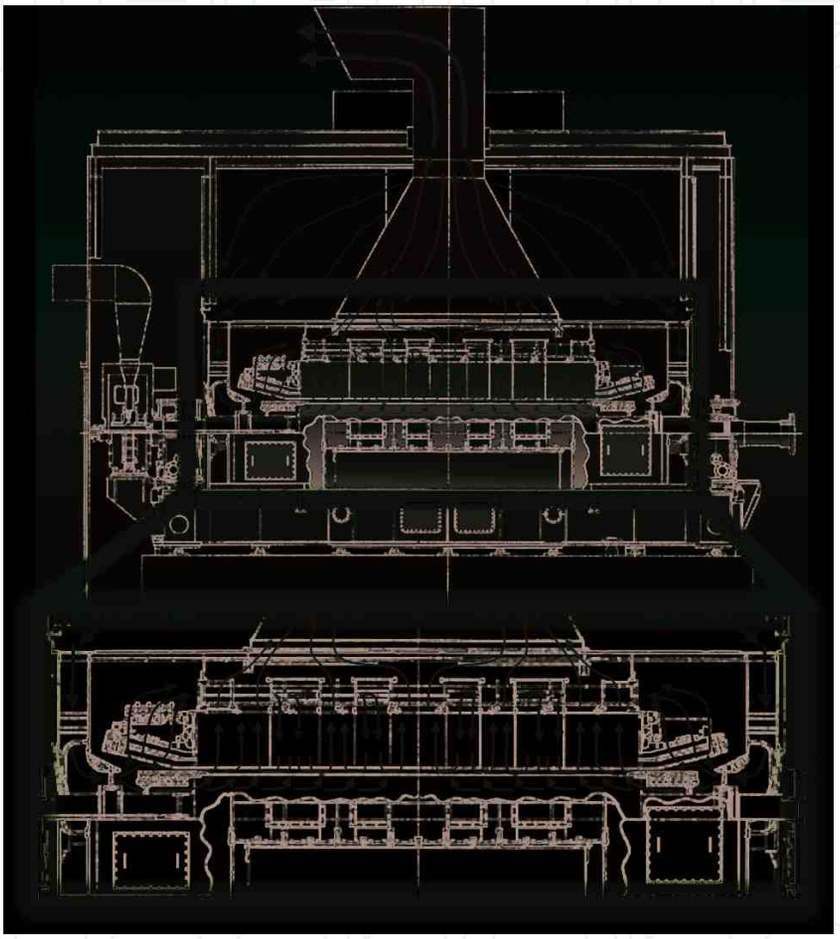

Figure 15. At left, the vibration sensing cavity housed inside a PEEK package. At right, the in-slot vibration sensor bandwidth can even be extended from 10 Hz~1 kHz (standard) to 5 Hz~2 kHz. Courtesy of QPS Photronics.

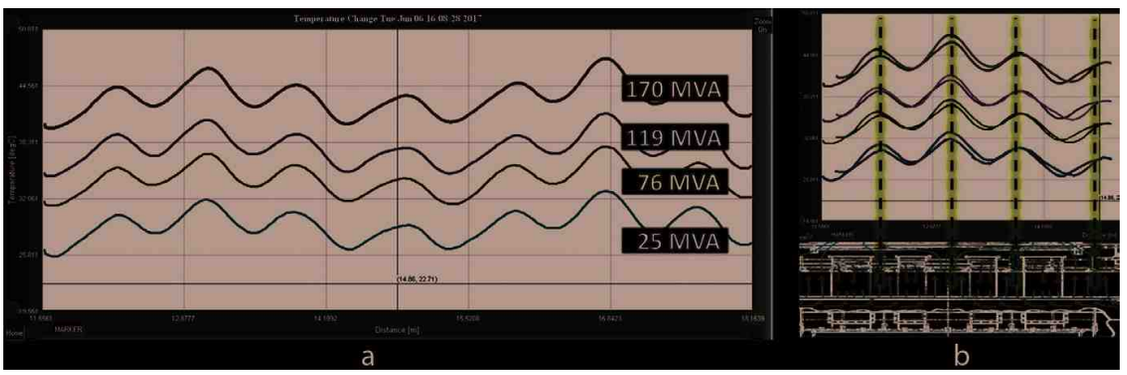

Figure 16. FFT shows in-slot vibration characteristics. Courtesy of QPS Photronics.

4.2.2. End winding lead vibration

One single point vibration sensor was installed at the end winding of the neutral lead as depicted in **Figure 17**. The photograph at the right shows the end winding conductor before installation where the colored circles pinpoint where the two additional discrete sensors would end up coupled.

The end winding lead sensor also showed strong vibration spectrum in both 1xLF and 2xLF. There were hardly any harmonics. The 1xLF component measured 15-mil peak-to-peak and the 2xLF component measured 11-mil. They are higher than what we expect but consistent to the in-slot measurement (see **Figure 18**).

4.2.3. End winding bus vibration

A third vibration sensor was mounted on the neutral end winding bus (see **Figure 17**). Once again, the vibration observed here is also consistent as depicted below in **Figure 19**.

Larger vibration amplitude is shown: 1xLF component measured 16.5-mil peak-to-peak and 2xLF measured 12.1-mil peak-to-peak. It seems that gas-fired generators vibrate much more than the coal-fired generators. Plant experts informed all participants of the field test that it may be related to the generator design where the bearing is coupled to the frame. Vibration was so strong in similar machines that cracks developed.

4.3. In-slot and end winding temperatures

The temperature distribution inside the slot was measured by the Brillouin fiber optic loop sensor. The gathered data brought up a wave-like distribution as demonstrated in **Figure 20**

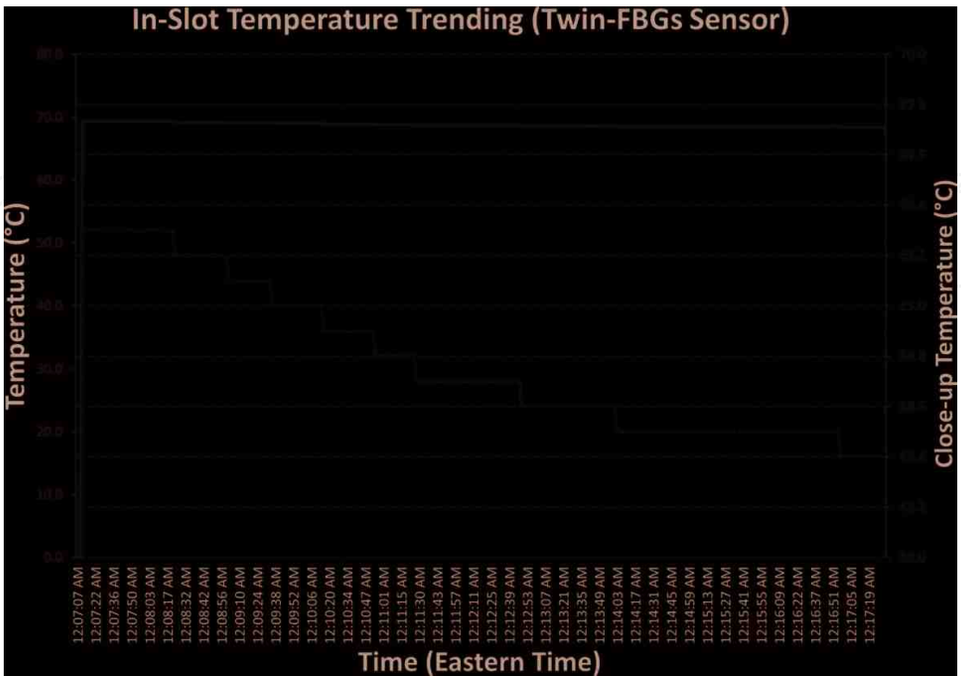

Figure 17. Two discrete sensors coupled at different locations of the neutral bus of the phase C conductor. Courtesy of Calpine Corporation and QPS Photronics.

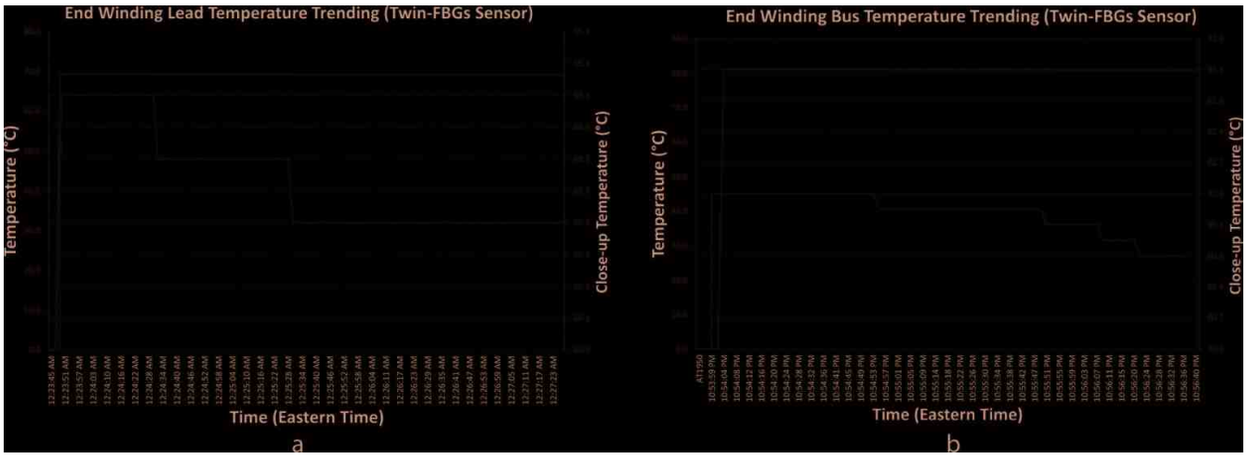

Figure 18. End winding lead frequency domain. Courtesy of QPS Photronics.

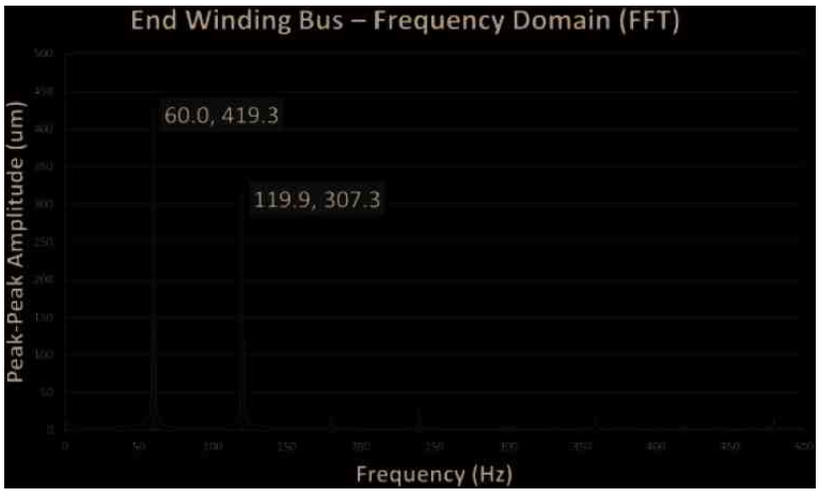

Figure 19. End winding bus frequency domain. Courtesy of QPS Photronics.

(left). The distribution is not flat; the cooling airflow did not form a perfect balance. The temperature extrema were less than 2°C apart, positively assuring the lack of hot spots.

We tried to line up the temperature profile with the layout of the air ducts by wrapping over at the middle. Valleys coincide very well with the air duct exhaust and the top peak always occurs in the middle between two air ducts where there is minimum cooling airflow as illustrated in **Figure 20** (right). The difference between peak and valley is consistent at different loading levels.

Figure 21 shows the temperature measurement of the in-slot sensor. The red plot indicates the coarse temperature reading of 70°C at a loading of 170 MVA. The blue line shows the fine temperature variation over a period of 10 min. The sensor was able to detect temperature changes down to 0.1°C.

The end winding lead of **Figure 22** (left) showed a temperature consistent with the slot as well as the end winding bus plotted in **Figure 22** (right). All of them read close to each other, there does not seem to be any problem.

http://dx.doi.org/10.5772/intechopen.78065

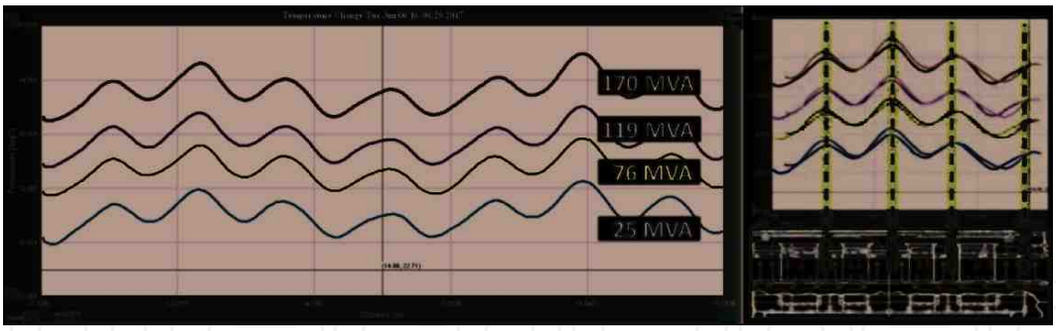

Figure 20. At left, temperature profiles at different loading intensities. At right, temperature profile line-ups with the air duct locations. Courtesy of Oz Optics, Ltd.

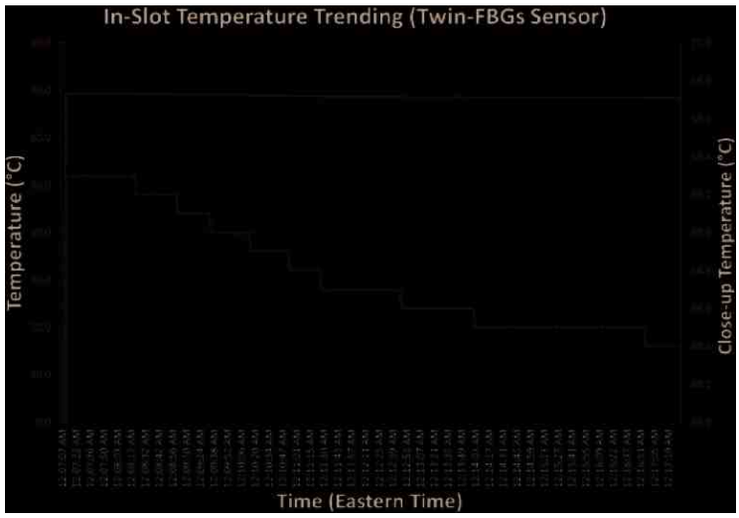

Figure 21. In-slot temperature measurement for 10 min. Courtesy of QPS Photronics.

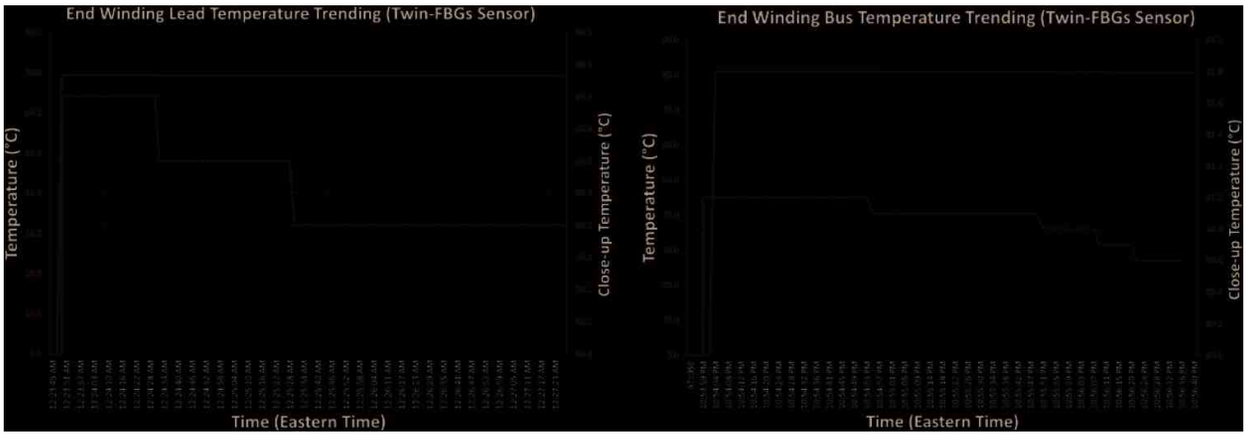

Figure 22. At left, end winding lead temperature measurement for about 5 min. At right, end winding bus temperature measurement for about 3 min. Courtesy of QPS Photronics.

4.4. Air cooling inside a gas-fired generator

The gas-fired generator involved in the field test was manufactured by Siemens [35–38]. **Figure 23** shows a conceptual diagram of the cooling air radial flow. There are resistance

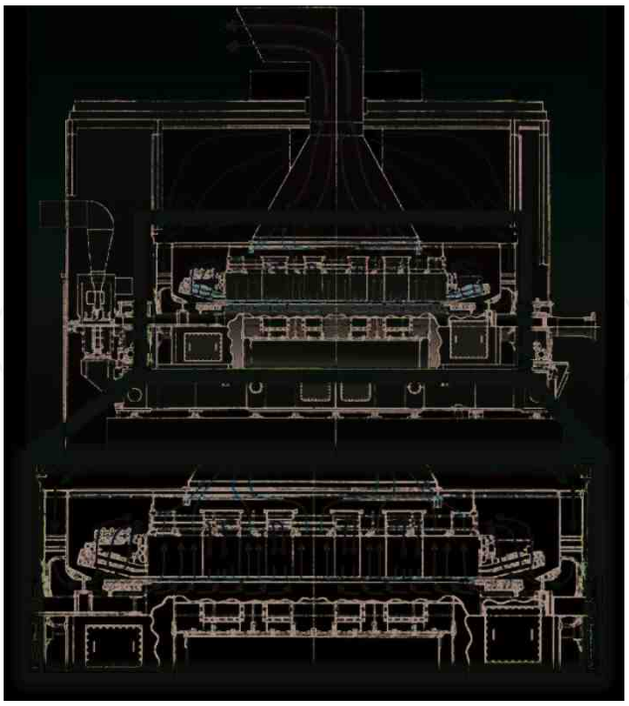

Figure 23. Siemens Westinghouse AeroPac I generator with emphasis on the radial airflow via colored arrows. Courtesy of Calpine Corporation.

temperature detectors (RTDs) installed at different locations along the air path. We will compare our measurement with those coming from the supervisory control and data acquisition (SCADA).

Cooling air flows through many cooling ducts placed approximately 2 inches apart from each other. Blue arrows are meant to represent cooler air entering the core. As it flows through the ducts, the air progressively relieves the stator core of its heat (yellow arrows) and it ends up evacuated (red arrows) via the main central exhaust. Since RTDs carry conducting material, they are mainly installed in the grounded core. This field test represented the first time where in-slot vibration and hot spot measurements were performed.

5. Analysis and discussion for temperature measurement

The field test was performed after a successful rewind. A close examination of a sample segment of the old winding showed that defects always started extremely small at the scale of few millimeters as seen in the pinholes of **Figure 6**. In the advanced stages of disturbance, there appears a single or multiple small dark depressions inside the exposed mica. These might represent two stages of degradation. If hot spots were to start as point defects, prior observations make sense. These disturbed areas in the carbon paint grew increasingly larger together with the dark spots within them. We could not confirm whether these dark spots represent complete shorts to the copper conductor. The mica insulation is usually quite thick. The dark spot certainly looks like a reduced thickness in the mica. This must be a lengthy process for the electro-etching caused by the plasma of deionized air resulting from a strong in-slot vibration

as mentioned in an earlier section of this paper. Discussion with the plant technical staff experienced with maintaining these gas-fired generators indicated that troubles seem to start typically after 5–10 years. The distributed temperature sensing Brillouin technology is usually used for oil and gas pipeline and helps to locate small leaks. Best spatial resolution is listed as three centimeters [39], which is much larger than the defects we observed, therefore, no hot spots were found despite our expectations. Given that the generator has been rewound and the insulation is new it would take several years for the defect to grow to a size large enough to be detected by the sensing fiber. We believe it is better to maintain the sensors as a continuous monitoring tool where we can see slight temperature changes down to 0.01°C increments.

5.1. Analysis and discussion for vibration measurement

This field test demonstrates consistent strong vibration in both 1xLF and 2xLF. A spectral analysis tool published by SKF USA Inc. [40], the strong vibration is related to misalignment (strong 2xLF amplitude) and also imbalance (strong 1xLF amplitude). Misalignment can be caused by thermal expansion; alignment could be performed when the generator is cold then heat up when it is placed in full operation. Thermal expansion might have caused the rotor to become elliptical instead of being perfectly circular. Misalignment could also be caused by shifting of the foundation or uneven support [41]. On the other hand, imbalance seems to be the cause of the strong 1xLF vibration. Their relative amplitude might indicate the extent of each problem (see [20]).

Referring to **Figure 15** of SKF USA Inc. article (see [40]), their example can be compared to the data of this field test (see **Figures 16**, **18** and **19**) and it seems that both imbalance and misalignment could be affecting the generator. These measured values were two to three times higher than typical measurements on large coal-fired generators. Those large generators do not display any 1xLF vibration signal at all because they are physically much larger in structure.

5.2. Proposed composite damage model for gas-fired generators

The fiber optic signal processing system equipped with a gateway device connects the large volume of sensor data with the plant data from the SCADA for parametric correlation between cause (loading, start-stop periods, etc.) and result (level of vibration and temperature). **Figure 24** displays a flowchart of damage diagnostic that would be further quantified with aforementioned correlation.

It is now possible to simplify the problem into an intuitive model that does not involve complex mathematics [42–46]. The methodology is described below and can be used to analyze the measured data from these fiber optic sensors. It has been known that gas generators are frequently subjected to many daily start-stop events: the winds are usually stronger during the night and the sun shines more strongly late morning and afternoon. When these renewable energies become abundant, gas turbines must be turned off for the total power to not overload the power grid (see **Figure 25**).

When these start-stop cycles occur [47], the inside temperature of a generator would go through significant changes. Frequent start-stop cycles together with strong vibration will potentially cause delamination of the insulation as well as voids at their interface with the conducting copper. They also have different coefficients of expansion. Severe vibration can

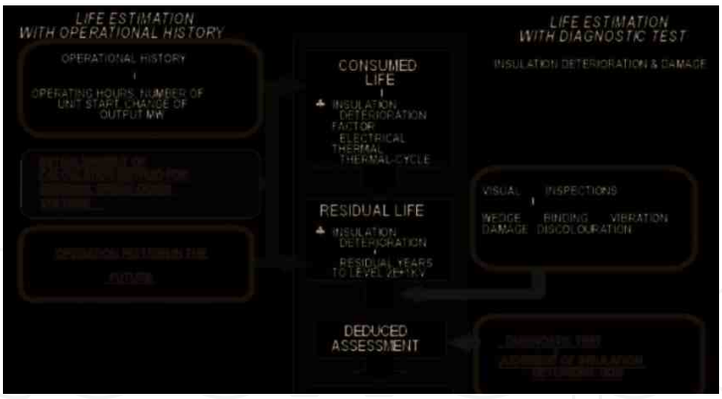

Figure 24. Damage model that allows residual life predictions.

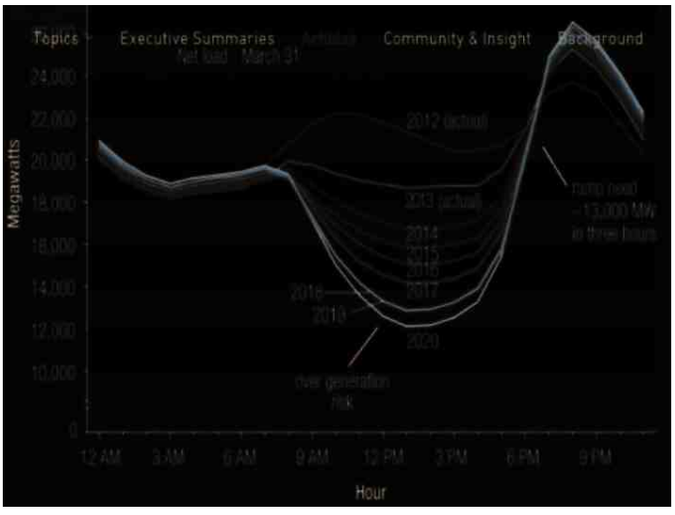

Figure 25. Graph showing gas generators must be turned on and off to adapt to the supply of the renewables.

introduce cracks inside the thick epoxy mica and voids inside the mica facilitating PDs [48–56]. Of course, winding temperature would depend on load which will show up in the temperature trending profile in an online monitoring configuration. Loading changes will be reflected in changes in the 2xLF vibration amplitude, which is affected by the electromagnetic forces interaction between the rotor and the stator. Simultaneously, the temperature will also see small adjustments due to additional heating caused by higher load currents. Hence, smaller temperature changes will reflect the loading conditions and correlation with the control signal from the SCADA system becomes unnecessary. Current stage of sensor development allows the freedom to take advantage of the latest technology like the internet-of-things (IofT) where signals can be analyzed by gateway devices attached to our signal processing system. Then, the partially analyzed data are transmitted to a cloud where higher level calculation is performed to form a residual life model as well as providing warnings for urgent attention and quick remedial decisions. As for the start-stop cycles, they will simply switch the vibration signals on and off. These will be very clear and easy to interpret. Since temperature change is slow, its decrease will come gradually. Again, these data can be derived without any connection to the SCADA system of the power plant (power industry is known to be very concerned about external connection to their SCADA, making it open to external hacking).

The proposed model consists of a menu of degradation processes, individually selectable to form a clear picture of health of the air-cooled gas-fired generator, all based on the sensor ability to work inside high voltages, and strong electromagnetic fields. They are also small (0.5″ X 3″ X 0.08″) and can fit inside the stator slots which are approximately 1″ in width. Once installed in place, these sensors will be able to measure both thermal as well as mechanical stresses. The class of insulation material and the operating voltage of the generator have defined the limit of the electrical stress. Thermal stresses can be measured directly inside the slot as well as the end winding overhang where curvature might give rise to current crowding. These sensors are also designed to be thin; they can easily conform to any curved surface yet maintain good thermal contact. The field test described in prior sections represents the first occasion where direct measurement could be done inside the generator slot. Previous work combining the total aging effect consider vibration as related mainly to fatigue, which might not be the case here.

From the failure analysis of the extracted winding section prior to the rewind, there was clear evidence of vibration sparking. Defects first appeared as small pinholes in the carbon paint, which grew with time. Once these defects grew into sufficient size while developing local high voltage spots, they cause the air to break down into plasma, whereas the remaining half of the vibration cycle broke the current path and turns the plasma into a source for electro-etching. Vibration sparking together with frequent start-stop cycles drastically shortens the lifespan of the gas-fired generator. This hypothesis was reinforced while working with Calpine maintenance staff: gas-fired generators typically start to have trouble as early as the warranty period within 5–10 years. This information is compared to the prior field tests of coal-fired base load generators monitoring stator end winding (SEW) vibration, where rewind would only be done after 30–40 years of operation. Vibration sparking might come with a threshold related to vibration peak-to-peak amplitudes. In fact vibration amplitudes observed at Hermiston field test showed a magnitude two to three times greater than the ones collected from coal-fired power plants where they are usually less than 150 microns peak-to-peak. There is another possibility. Large coal-fired generators are hydrogen-cooled. Hydrogen does not break down easily, pinhole defects in their old winding samples were rare occurrences. The proposed second field test for Calpine Corporation will take place in their plant of Texas (Hidalgo Energy Center) where the gas-fired generator would be hydrogen-cooled. We will go through the same analysis and compare the vibration and temperature data there. Fiber optic sensor capturing PD events will be introduced, provided PD first produced the pinhole defects that facilitated the following vibration sparking destruction. Those PD sensors are based on a very long FBG cavity. Cavity length affects sensor performance: the longer the cavity, the denser would be the interference fringes. These fringes will have steeper slopes and therefore more sensitive to small surface acoustic wave perturbations. Fringes are so densely packed spectrally that maintaining the operating point will not be needed. This PD sensor will not be affected by small changes in temperature and will pick up PD events along the full length of the optical fiber cavity. However, it is a dedicated PD sensor and will not be able to measure temperature. The distributed low frequency vibration sensor will be set in the same slot as the PD sensor to collect all the data that would complement each other.

The influence of PD on the proposed aging model is that they start to register pinhole formation. As the defects grew both in magnitude and incidence, an indication is given about the size of the carbon paint disturbance. However, the PD sensor would not be able to detect the

Figure 26. Cracking of copper turns and also bowing of the rotor.

onset of electro etching. Arcing experiments will be conducted in laboratory environment to study and relate the signatures associated with the electro-etching process.

In summary, it is a damage model of the insulation. It is related to the accelerated aging of insulation inside the gas-fired generator and additional work will be needed to turn it into a residual life prediction model. Such a model will depend on the design, and manufacturing workmanship, which vary depending on the individual OEMs.

5.3. Influence of start-stop cycles

Frequent start-stop cycles can cause stresses due to coefficient of expansion differences between different materials used inside the generator (see **Figure 26**).

In the industry, the effect of start-stop cycles is introduced as a life consumption factor. Attempts to use the gas generator to compensate for the intermittent renewables like the solar and wind is one instance. It might have to be turned on and off several times per day. The number of times per day serves to cause an apparent acceleration factor. In a case where it is done three times a day, each additional day of operation in that fashion is equivalent to 3 days of operation, effectively shortening their lifespan. An increasingly accumulated number of start-stop cycles per day correspondingly shorten the life of the generator. This explains the difference between the expected onsets of problems comparing a coal-fired power plant versus the gas-fired unit. Coal-fired plants usually need to be rewound after 30 years, whereas the gas generator needs adjustments at a daily pace depending of the wind and solar, leading to a major maintenance even inside the warranty period. This aging factor ranges from three to six, depending on the frequency of start-stop cycles per day.

So the life of a gas generator depends not only on who manufactured them, but it also depends how owners use them. Using fiber optic sensors it would be possible to get a real-time picture of how the generator is doing and extend its lifespan.

In summary, a new class of fiber optic sensors is introduced and can address the following complex problems:

- Marginal design and poor choice of material to be indicated by the onset of PD activities
- Number of start-stop cycles in its mode of operation as observed in the cycle of large temperature changes

http://dx.doi.org/10.5772/intechopen.78065

- Ongoing electrical and thermal stresses
- Degradation due to vibration sparking
- Signature analysis of the observed vibration spectrum indicating structural looseness and other mechanical problems like misalignment and unbalancing.

With the upcoming field tests, this aging model covering generators of various sizes and make will become more sophisticated, turning the monitoring solution into a service business.

6. Conclusion

Sensors which can survive in a hostile environment are essential to understanding the aging process of turbines. It is quite possible that the key to extending the lifespan of turbines is real time monitoring using fiber optic sensors for both vibration and temperature.

We have proven through this test that real time monitoring of vibration and temperature is both possible and economical. What needs to happen now is that these measurements need to take a part in the day to day operation of generating plants. By sensing internal vibration and temperature we can know when a particular turbine is on the edge of conditions which will lead to lasting damage and a control scheme can be implemented where other turbines will start up to alleviate those conditions before damage happens resulting in increased life span of all the turbines. At the moment these turbines have a very limited lifespan, typically 7 or 8 years. With improved controls there could be a significant improvement in that lifespan. This would have benefits in reducing asset costs, improving reliability to customers and improved safety for workers at the plant.

Acknowledgements

The authors would like to express gratitude to Calpine Corporation for allowing and facilitating the installation of the fiber optic sensing systems at the Hermiston Power Project plant. Likewise, contribution from Oz Optics, Ltd. is highlighted for providing temperature records from their Brillouin distributed temperature technology. At last, acknowledgements are given to the senior consultant George F. Dailey for bringing all participants together and Refined Manufacturing Acceleration Process (ReMAP) network for providing a substantial financial aid.

Author details

Peter Kung

Address all correspondence to: peter@qpscom.com

QPS Photronics Inc., Canada

References

[1] Maughan C. Premature failure of modern generators. Proceedings of 20th International Conference on Nuclear Engineering; July 30-August 3 2012; Anaheim, California: pp. 866-870. DOI: 10.1115/ICONE20-POWER2012-54584

[2] Barré O, Napame B. The insulation for machines having a high lifespan expectancy, design, tests and acceptance criteria issues. Machines. Feb. 2017;**5**(1):7. DOI: 10.3390/machines5010007

[3] Ge J, Qiu C, Xie H. Partial Discharge Measurements[M]. Beijing: China machine press; 1984

[4] Stone GC, Wu R. Examples of Stator Winding Insulation Deterioration in New Generators. DOI: 10.1109/ICPADM.2009.5252475

[5] Morshuis PH. F partial discharge mechanisms in voids related to dielectric. Degradation IEE Proceedings–Science, Measurement and Technology. 1995;**142**(1):62-68

[6] Brutsch R, Tari M, Frohlich K, et al. Insulation failure mechanisms of power generators. IEEE Electrical Insulation Magazine. 2008;**24**(4):17-25

[7] Jiang Q. Research on UHF Detection Technology of Partial Discharge in Power Transformer [D]. Baoding: North China Electric Power University; 2006

[8] Stone GC. Deterioration of Stator Winding Insulation by Vibration Sparking. Proceedings of 2008 International Symposium on Electrical Insulating Materials, Yokkaichi, Mie, Japan, September 7-11, 2008. pp. 171-174. DOI: 10.1109/ISEIM.2008.4664445

[9] Xie H. Electrical Insulation Structure Design Principle. Beijing: Machinery Industry Press; 1993

[10] Wu S, Xie D, Chen S, Yu B. Electrical Insulation Materials and Engineering. Xi'an: Xi'an Jiaotong University Press; 1996

[11] Kako Y, Tsukui T, Mitsui H, Hirabayashi S, Kimura K, Natsume F. The process of electrical strength and insulation aging for the system of HV motor. Foreign Electrical Machinery. 1989;**3**:52-57

[12] Wang S. The formation characteristics and development of common generators insulation faults. Large Electrical Machinery Technology. 1987;**6**:25-29

[13] Lei Q. Structure and Electrical Properties of Polymer. Wuhan: Huazhong University of Science and Technology Press; 1990

[14] Iike M, Tsujimura T, Muraoka M. Life diagnosis of epoxy resin coil insulation system. Fuji Electric Journal. December 1989;**62**:12

[15] Wang S, Zhou D. Operation Characteristics and Test of Large Generator Insulation. Beijing: Machinery Industry Press; 1992

[16] Tshiloz K, Smith AC, Mohammed A, Djurović S, Feehally T. Real-time insulation lifetime monitoring for motor windings. Proceedings of International Conference on Electrical Machines, ICEM. 2016. pp. 2335-2340. DOI: 10.1109/ICELMACH.2016.7732847

[17] Hydro A. Generator Winding Insulation [Internet]. 2011. Available from: http://www.nwhydro.org/wp-content/uploads/events_committees/Docs/2011_Tech_Workshop/GeneratorWinding-Heaton.pdf [Accessed: 2018-02-07]

[18] Niikura H, Inoue S, Yamazaki M. Global vacuum pressure impregnation insulation applied to hydrogen-cooled generators. Fuji Electric Review. 2009;**55**(3):93-98

[19] Kung P, Wang L, Comanici MI. Stator end winding vibration and temperature rise monitoring. Electrical Insulation Conference (EIC). June 2011. pp. 5-8. DOI: 10.1109/EIC.2011.5996105

[20] Wan S, He Y. Investigation on stator and rotor vibration characteristics of turbo-generator under air gap eccentricity fault. Transactions of the Canadian Society for Mechanical Engineering. 2011;**35**:161-176

[21] Oliquino R, Islam S, Eren H. Effects of types of faults on generator vibration signatures. Australasian Universities Power Engineering Conference (AUPEC2003). 2003. pp. 1-6

[22] Djurović S, Vilchis-Rodriguez D, Kung P, Comanici MI, Smith AC. Investigation of induction generator wide band vibration monitoring using fibre Bragg grating accelerometers, Proceedings of International Conference on Electrical Machines, ICEM 2014. pp. 1772-1778. DOI: 10.1109/ICELMACH.2014.6960423

[23] Mohammed A, Djurovic S, Smith CA, Tshiloz K. FBG Sensing for Hot Spot Thermal Monitoring in Electric Machinery Random Wound Components. Proceedings of International Conference on Electrical Machines, ICEM 2016. DOI: 10.1109/ICELMACH.2016.7732837

[24] Kung P, Comanici MI, Li Q, Zhang Y. Development of a long-gauge vibration sensor. Proceedings of SPIE–The International Society for Optical Engineering. 2015. p. 9359. DOI: 10.1117/12.2076068

[25] Cygan P, Laghari JR. Models for insulation aging under electrical and thermal multistress. IEEE Transaction on Electrical Insulation. 1990;**25**(5):923-934

[26] Shi J, Yang Y. Study on fault characteristics of large turbo generator. Proceedings of the CSEE. 2000;**20**(7):44-47

[27] Jing S. Design of Main Insulation Aging Multi Factor Test System for Large Motor and Research on Aging Property of Stator Bar[D]. Harbin: Harbin University of Science and Technology; 2011

[28] Raman TS. Degradation of HV generator insulation mechanical, electrical and thermal stresses. IEEE International Symposium on Electrical Insulation, Toronto, Canada, June 1990. pp. 21-24. DOI: 10.1109/ELINSL.1990.109699

[29] Feng D. Research on New Fiber Bragg Grating Sensor [D]. Taiyuan: Northwest University; 2016

[30] Kersey D, Patrick HJ, LeBIanc M, et al. Fiber grating sensors. Journal of Lightwave Technology. 1997;**15**(8):1442-1463

[31] Othonos A, Kalli K. Fiber Bragg Gratings. London: Artech House, ISSN: 0342-4111,1999

[32] Griscenko M, Vitols R. Stator core vibration and temperature analysis of hydropower generation unit at 100 Hz frequency. In: proceedings of 14th International Scientific Conference. Jelgava, Latvia. May 20-22, 2015. pp. 383-388

[33] VibroSystM. On-line vibration and temperature direct measurement on high voltage devices using fiber optic sensor technology. In: CMD Conference Proceedings. 2010

[34] Srinivas MB, Ramu TS. Multifactor aging of HV generator stator insulation including mechanical vibrations. IEEE Transactions on Electrical Insulation. 1992;**27**(5):1009-1021

[35] Westinghouse Electric Corporation. Installation Operation Maintenance Instructions: Air-Cooled Turbine Generators 1000 to 7500 kW. East Pittsburgh, PA: Author; 1947 Available from: http://www.electricalpartmanuals.com/manual/air-cooled-turbine-generators-1000-to-7500-kw

[36] Energy GE. Generator In-Situ Inspections – A Critical Part of Generator Maintenance Cost Reduction. Schenectady, NY: Markman C & Zawoysky R J; 2012 Available from: https://www.gepower.com/content/dam/gepower-pgdp/global/en_US/documents/technical/ger/ger-3954c-generator-in-situ-inspections.pdf

[37] Hattori K, Takahashi K, Tohnosu S, Miyakawa K. State-of-the-art technology for large turbine generators. CIGRE SC A, 1, 2008; 2008

[38] Siemens. Generator Upgrades and Modernization. Ruhr, Germany: Michal Gawron; 2015. Available from: http://www.siemens.fi/pool/cc/events/160years-vip-seminar/gawron.pdf

[39] Oz Optics Ltd. Fiber Optic Distributed Temperature Sensors (B-DTS). 2018. Available from: https://www.ozoptics.com/ALLNEW_PDF/DTS0127.pdf

[40] SKF USA Inc. 2002. Spectrum Analysis – The Key Features of Analyzing Spectra (CM5118). Available from: http://www.skf.com/binary/tcm:12-113997/CM5118%20EN%20Spectrum%20Analysis.pdf

[41] VESKi d.o.o. CASE STUDY-07 Loose Bearing to Foundation Support/Portable Diagnostic System. Available from: http://www.veski.hr/public/brochures/Case%20study%2007%20TG%20Loose%20bearing.pdf

[42] Zhe H. Modeling and Testing of Insulation Degradation Due to Dynamic Thermal Loading of Electrical Machines [Thesis]. Lund: Division of Industrial Electrical Engineering and Automation, Faculty of Engineering, Lund University; 2017

[43] Adawi S, Rameshkumar G. Vibration diagnosis approach for industrial gas turbine and failure analysis. British Journal of Applied Science & Technology. 2016;**14**:1-9. DOI: 10.9734/BJAST/2016/23163

[44] Twiddle J, Muthuraman S, Connolly N. Condition Monitoring of the SSE Generation Fleet. Journal of Physics Conference Series (Online). May 2012;**364**(1):1-12. DOI:101088/1742-6596/364/1/012104

[45] ABB Brazil. LEAP-life expectancy analysis program. For Electrical Rotating Machines. 2006. Santiago, Chile: Marcio gennari. Available from: http://www02.abb.com/global/clabb/clabb151.nsf/0/588c647ab96ec0fdc12571f00064d269/$file/MAPLA+2006+-+ABB+Marcio+Gennari+Presentation.pdf

[46] ABB Group. Stator Winding-Condition & Lifetime Assessment. 2013. Available from: http://www02.abb.com/global/zaabb/zaabb011.nsf/bf177942f19f4a98c1257148003b7a0a/71d80922c9b6b63ac1257b7200343c9b/$file/dmmg+6+-+abb+leap+stator+winding-condition+and+lifetime+assessment.pdf

[47] Kokko V, Ahtiainen J. Ageing Due to Start-Stop Cycles and Frequent Regulation in Lifetime Estimation of Hydro Turbines and Generators. Grenoble, April. 2014: 9-11

[48] Kung P, Qin Z, Li W, Bao X. Using Distributed Sensing for Generator Condition Monitoring. 2013. Available from: http://www.hydroworld.com/articles/hr/print/volume-32/issue-7/articles/using-distributed-sensing-for-generator-condition-monitoring.html

[49] Robles E. Field Diagnostic Testing of Power Generators and Transformers Using Modern Techniques. Paper No. 12 presented at HV Testing, Monitoring and Diagnostics Workshop 2000, Alexandria, Virginia, USA, 13 & 14 September 2000. pp. 1-6

[50] Harjo S. Partial discharge in high voltage insulating materials. International Journal on Electrical Engineering and Informatics. 2016;**8**:147-163. DOI: 10.15676/ijeei.2016.8.1.11

[51] Rao B. Assessment of stator winding insulation by spectroscopic and thermo analytical techniques, PART 1-Review of deterioration mechanisms and condition monitoring techniques. The Journal of Central Power Research Institute. 2009;**5**:2. ISSN 0973-0388

[52] Li R, Pan L, Yan C, Li H, Hu B. Condition evaluation of large generator stator insulation based on partial discharge measurement. Advances in Mechanical Engineering. 2013;**5**. DOI: 10.1155/2013/765374

[53] Clemmons S. Continuous, On-Line PD Monitoring for Generators. 2017. Available from: http://www.power-eng.com/articles/print/volume-121/issue-10/features/continuous-on-line-pd-monitoring-for-generators.html

[54] Ruihua L, Pan L, Yan C, Li H, Hu B. Condition evaluation of large generator Stator insulation based on partial discharge measurement. Advances in Mechanical Engineering. 2013;**2013**. DOI: 10.1155/2013/765374

[55] ReliaSoft Corporation. Accelerated Life Testing Reference. 2015. Available from: http://www.synthesisplatform.net/references/Accelerated_Life_Testing_Reference.pdf

[56] Luo Y, Li Z, Wang H. A review of online partial discharge measurement of large generators. Energies. 2017;**10**:1694. DOI: 10.3390/en10111694

IntechOpen